Science Press

ARTICLE

Effect of Welding Thermal Cycle and Peak Temperature on Microstructure of C-HRA-2 Nickel-Based Alloy

Kou Dongxu[1], Chen Zhongyi[1], Chen Zhengzong[2], Li Yongqing[3], Ma Yonglin[1], Li Yiming[1,4]

[1] School of Materials and Metallurgy, Inner Mongolia University of Science and Technology, Baotou 014010, China; [2] Institute for Special Steels, Central Iron and Steel Research Institute Co., Ltd, Beijing 100081, China; [3] Technology Center, Inner Mongolia North Heavy Industries Group Co., Ltd, Baotou 014033, China; [4] Key Laboratory of Advanced Metals and Materials of Inner Mongolia, Inner Mongolia University of Science and Technology, Baotou 014010, China

Abstract: The welding heat-affected zone (HAZ) of C-HRA-2 nickel-based alloy under various primary peak temperatures (T_{p_1}=1150, 1250, and 1350 °C) and the secondary peak temperatures (T_{p_2}=850, 950, 1050, 1150, 1250, 1350, and 1450 °C) was obtained by welding thermal simulation. The effect of peak temperature (T_p) and thermal cycling times on the evolution of simulated HAZ microstructure of C-HRA-2 alloy was investigated. The microhardness of simulated HAZs was measured. The HAZ microstructure and carbide were characterized by the optical microscope, scanning electron microscope, and transmission electron microscope. Results show that the fine $M_{23}C_6$ carbides appear along the grain boundaries in the simulated HAZ with T_{p_1}=1150 °C. For HAZs with T_{p_1}>1250 °C, the γ matrix bonded with $M_{23}C_6$ carbides appears near the grain boundaries due to component liquefaction. When T_{p_2} is 1050–1250 °C, the carbides similar to those in HAZ with T_{p_1}=1150 °C can be observed near the grain boundaries due to the difference in the solid solubility of Cr in the matrix obtained at T_{p_1} and T_{p_2}. In HAZ with T_{p_2}>1250 °C, the melted microstructure similar to that with T_{p_1}=1250 °C can be observed near the grain boundaries. The microhardness fluctuates significantly with increasing the T_{p_2}. The microhardness of specimen with T_{p_2}=1250 °C is slightly higher than that of the base material, because of the grain boundary strengthening effect of the carbides near the grain boundaries.

Key words: C-HRA-2 alloy; welding thermal simulation; microstructure evolution; $M_{23}C_6$ carbide

C-HRA-2 alloy is a pure solution-reinforced heat-resistant Ni-Cr-Co-Mo alloy with face-centered cubic structure, which is usually used for large-diameter and thick-walled tubes, such as boiler collectors and main steam pipes of ultra-supercritical power stations, serving at 650–680 °C[1–2]. The weldability and welding process are crucial for the practical application of C-HRA-2 alloy. In the welded joint of the material, the microstructure of the weld metal and heat-affected zone (HAZ) is usually different from that of the base metal (BM), which may affect the mechanical properties and reliability of the welded joint[3]. Therefore, the research on the mechanical properties of welded joints is important.

HAZ simulation can quickly and accurately distinguish the weakest point of the welded joint, thus attracting much attention for the investigation of structural changes in HAZ[4–5]. Multi-pass welding is a commonly used treatment, so the simulated thermal cycle is usually set as two or more passes. Generally, the heat source of subsequent passes will have an impact on the previously formed HAZ. Therefore, HAZ suffers from repeated welding thermal cycles, resulting in complex and different microstructures and mechanical behavior. The microstructures and mechanical properties of alloy after single-pass welding are significantly different from those after multi-pass welding[6–10]. Shao et al[11] conducted the welding thermal simulation of HAZ in high chromium ferritic steel after double-pass welding, and found that the double-pass thermal cycling can cause austenite grain refinement, and $M_{23}C_6$ carbides are firstly coarsened and then dissolved with

increasing the secondary peak temperature T_{p_2}. Fu et al[12] conducted welding thermal cycling tests on 2.25Cr-1Mo-0.25V steel and found that the number of welding thermal cycles can influence the shape of precipitated phase. Zhu et al[13] conducted welding thermal simulation of Q690D steel by Gleeble thermal simulator and found that the microstructure is coarsened and the hardness is increased with increasing the peak temperature T_p during the welding thermal cycle. The hardness is further improved after the secondary thermal cycle, compared with that after the single-pass thermal cycle. Li et al[14–15] investigated the effects of peak temperature T_p, holding time, and the number of thermal cycles on the microstructure and mechanical behavior of $M_{23}C_6$ carbides in 617B alloy by thermal simulation. It is found that the holding time at T_{p_2} can affect the precipitation morphology of carbides. Jiang et al[16] studied the microstructure and hardness of 617B alloy after welding, and concluded that the re-solution of $M_{23}C_6$ carbides can strengthen the alloy after welding thermal cycles.

C-HRA-2 alloy is a kind of 617B alloy with ameliorated composition and without Al and Ti elements, so it does not contain γ' precipitation phase and can be used for welding without post-weld heat treatment, which greatly reduces the production cost. Chen et al[17–19] prepared the C-HRA-2 welding materials for medical application. Most reports focus on the composition optimization, thermal deformation behavior, microstructure evolution during long aging, enduring strength, and fatigue properties of C-HRA-2 alloy. Dong[20–22] and Zhou[23] et al studied the microstructure evolution and variation of mechanical properties of C-HRA-2 alloy after long aging at 675 and 700 °C. Results show that $M_{23}C_6$ carbides of C-HRA-2 alloy are coarsened with increasing the aging time, and the precipitation reaches the maximum after 3000 h. The strength, hardness, and toughness of the C-HRA-2 alloy are stabilized after aging at 675 °C for 500 h. However, the evolution of HAZ microstructure of C-HRA-2 alloy is rarely reported. Therefore, in this research, the effects of peak temperature T_p and the number of thermal cycles on the carbide formation, microstructure, and microhardness of C-HRA-2 alloy were investigated, providing theoretical guidance for further optimization of C-HRA-2 alloy during welding process.

1 Experiment

The experiment material was C-HRA-2 alloy (Central Iron and Steel Research Institute), whose chemical composition is shown in Table 1. The alloy specimens were obtained from the forged rod of C-HRA-2 alloy, then solution-annealed at 1150 °C for 1 h, and finally water-quenched. Since HAZ in multi-pass-welded joint is extremely narrow and heterogeneous, the effect of welding thermal cycles on the HAZ

microstructure can hardly be quantified. Therefore, the welding thermal simulations were conducted by L78 quench dilatometer to amplify HAZ. The specimen size for HAZ simulation was $\Phi5$ mm×10 mm. The microstructure analysis of specimens was observed by optical microstructure (OM), scanning electron microstructure (SEM, Super55), and transmission electron microstructure (TEM, JEM-2100). The mixed solution of $CuCl_2$ (1 g), HCl (20 mL), and CH_3CH_2OH (20 mL) was used to corrode the polished surface of specimen for 3.5 min, and then the microstructure was observed by SEM. The thin films were prepared by double-jet polishing in the mixed solution of 150 mL $HClO_4$ and 850 mL CH_3CH_2OH. The temperature was set as 25 °C and the voltage was set as 30 V. The microstructure and carbides were analyzed through selective area electron diffraction (SAED) to determine the phases. The chemical composition was measured by energy dispersive spectrometer (EDS). The Vickers hardness tester was applied to measure the specimen microhardness. The load was 100 g and the holding time was 15 s. Each specimen was measured six times and the average value was used for analysis.

The already-formed HAZ microstructure might be changed by the subsequent welding thermal cycles. Therefore, the microstructure and properties of the welded HAZ should be investigated to ensure the quality of welded joints. The thermal cycle simulation processes for HAZ during the single-pass thermal cycle with different peak temperatures were conducted to investigate the primary HAZ microstructure, as shown in Fig. 1a. Firstly, the specimens were heated from room temperature to 150 °C at heating rate of 10 °C/s, held for 60 s, then further heated to the peak temperatures (T_p=1150, 1250, 1350 °C) at heating rate of 200 °C/s, and held for 2 s. Afterwards, the specimens were cooled to 800 °C at cooling rate of 60 °C/s, then to 300 °C at cooling rate of 12 °C/s, and finally to room temperature at cooling rate of 2 °C/s. Fig. 1b and 1c show the simulated double-pass welding processes. The first peak temperature T_{p_1} was set as 1350 °C and the secondary peak temperature T_{p_2} was set as 850, 950, 1050, 1150, 1250, and 1350 °C. The heating and cooling rates of the double-pass welding were the same as those in the single-pass thermal cycle. The microstructure evolution of C-HRA-2 alloy at the higher T_p was also investigated: the welding thermal simulation with the first and the secondary peak temperatures of 1450 °C was conducted, and the resultant HAZ microstructure was observed by laser scanning confocal microscope. The thermal simulation process with higher T_p is shown in Fig. 1c. The specimen size was $\Phi3$ mm×1 mm. The Vickers hardness was applied to measure the microhardness of welded specimens. The mean diameter and distribution of grain size of each specimen were obtained by the Image-Pro Plus software.

2 Results and Discussion

2.1 BM microstructure

Fig. 2a and 2b show OM and SEM microstructures of BM,

Table 1   Chemical composition of C-HRA-2 alloy (wt%)

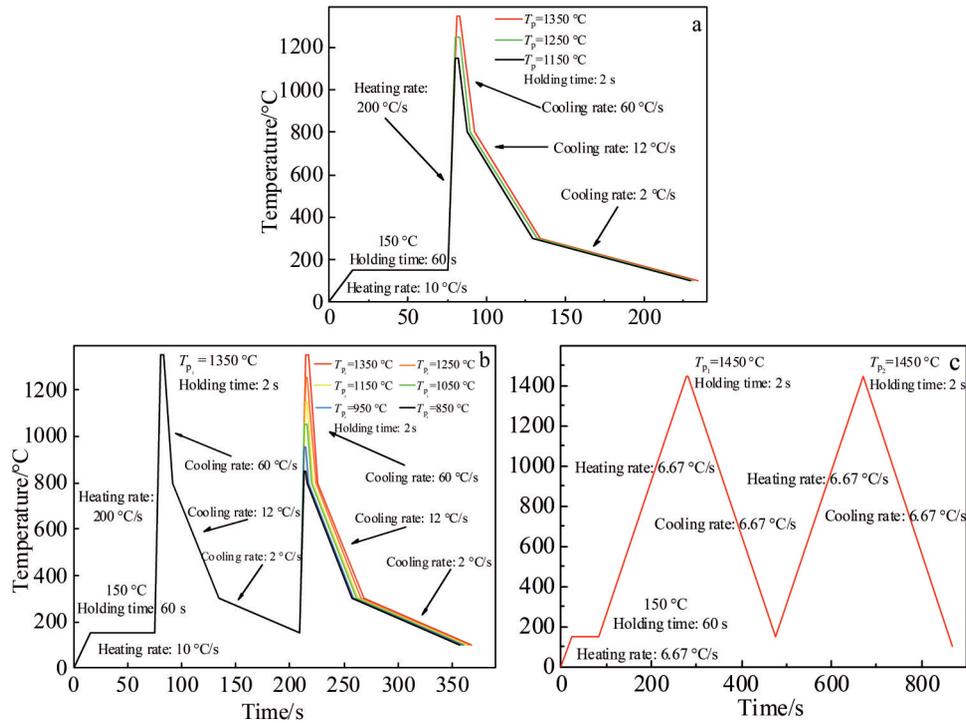| C	Nb	Si	Cr	Mo	B	W	Zr	Co	Ni
0.058	0.03	0.047	22.33	8.80	0.0057	0.21	0.013	12.1	Bal.

Fig.1　Thermal cycle simulation processes of HAZ during different welding passes: (a) single-pass welding with different peak temperatures; (b) double-pass welding with fixed first peak temperature and different secondary peak temperatures; (c) double-pass welding with fixed first and secondary peak temperatures
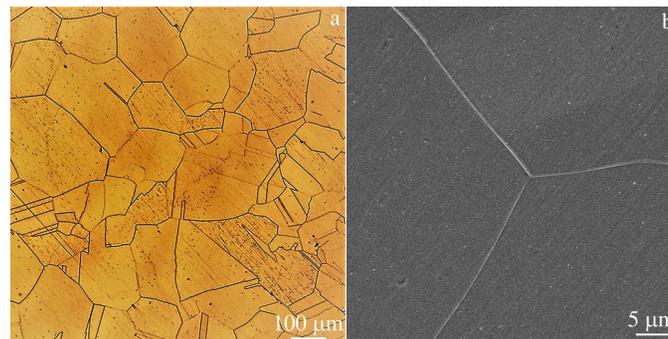

Fig.2　OM (a) and SEM (b) BM microstructures

respectively. The austenitic matrix and twin crystals with austenite grain size of 77–177 μm can be observed. Because BM is treated by solid solution, nearly all previously existed carbides are solid-solved into the matrix, thus resulting in the almost invisible carbides near the grain boundaries, as shown in Fig.2b. According to Ref.[1,20–21], the specimens undergo significant grain growth after solid solution treatment.

2.2　Thermal cycle simulation of single-pass welding

HAZ microstructures after single-pass welding with different peak temperatures are shown in Fig. 3. At T_p=1150 °C, many fine granular precipitates appear at the grain boundaries, as shown in Fig.3a. Fig.3b shows TEM microstructure of the C-HRA-2 alloy at T_p=1150 °C, and SAED pattern corresponding to the circle area in Fig.3b is shown in the inset

of Fig. 3b. It can be seen that the tiny particles precipitated along grain boundaries are $M_{23}C_6$ carbides with size of 100–200 nm. Both $M_{23}C_6$ carbides and the nickel-based γ matrix have face-centered cubic structure, and the lattice constant of $M_{23}C_6$ carbides is about three times larger than that of the γ matrix[24]. Fig. 3c and 3d show that the melted microstructures appear near the grain boundaries of the simulated HAZs at T_p= 1250 and 1350 °C. Large melted microstructure appears near the grain boundaries at T_p=1250 °C, whereas even larger pits appear under the liquefied microstructure, which may be caused by the migration of internal liquefied microstructure to the surface after solidification. This result indicates that the component liquefaction in C-HRA-2 alloy occurs above 1250 °C. EDS analysis results show that the slight difference
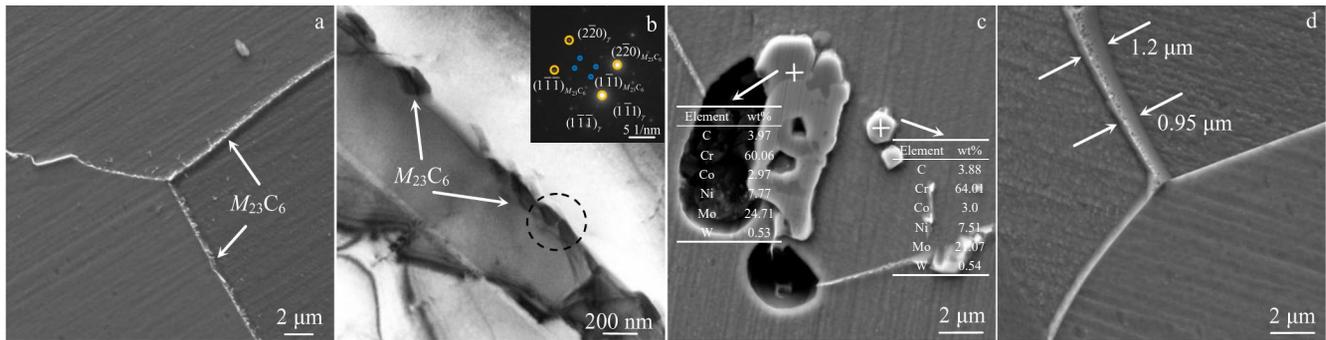
Fig.3   SEM microstructures and EDS analysis results of HAZ in C-HRA-2 alloy after thermal cycle simulation with single-pass welding of different peak temperatures: (a) 1150 °C, (c) 1250 °C, and (d) 1350 °C; TEM microstructure and corresponding SAED pattern to the circle area of HAZ in C-HRA-2 alloy after thermal cycle simulation with peak temperature of 1150 °C (b)

in composition at different locations is mainly caused by the diffusion and redistribution of atoms during the welding thermal cycles[25]. The grain boundaries have longer width in the simulated HAZ at T_p=1250 °C, which may be caused by the liquefaction of γ matrix structure near the grain boundaries.

2.3 Thermal cycle simulation of double-pass welding

Because the first peak temperature of 1350 °C is higher than the solid solution temperature (1150 °C), BM undergoes the solid solution again during the first thermal cycle. The microstructures near the grain boundaries after the secondary thermal cycle at different peak temperatures are shown in Fig.4. Usually, the fine particles near the grain boundaries are $M_{23}C_6$ carbides. However, no obvious $M_{23}C_6$ carbides can be observed near the grain boundaries when T_{p_2} is 850–950 °C, as shown in Fig.4a and 4b. Dong et al[1] found that the precipitation temperature range of $M_{23}C_6$ carbides in C-HRA-2 alloy is 898–1040 °C by Thermo-Calc software calculations. Therefore, no carbides are precipitated yet. The granular $M_{23}C_6$ carbides appear at the grain boundaries when T_{p_2}≥1050 °C, and the amount of $M_{23}C_6$ carbides is relatively large at the grain boundaries. The sizes of $M_{23}C_6$ carbides are similar to each other when T_{p_2}=1050–1250 °C. The particle size is 0.1–0.3 μm, but the particle densities are different, as shown in Fig. 4c – 4e. In addition to the granular particles near grain boundaries at T_{p_2}=1250 °C (Fig.4e), the melted microstructure is surrounded by some small particles, as shown in Fig. 4f. This microstructure is similar to that in the simulated HAZ after single-pass welding at T_p=1250 °C. EDS result indicates that the component mainly contains Ni, Cr, Co, and Mo. Li et al[14–15] reported that the eutectic microstructure is composed of γ matrix and $M_{23}C_6$ carbides due to the complicated welding thermal cycle.

The granular $M_{23}C_6$ carbides can barely be observed near the grain boundaries in the simulated HAZ at T_{p_2}=1350 °C. This is because the peak temperature is too high, resulting in the solid solution of 2 times for the matrix. Therefore, most alloying elements are solved into the matrix. When T_{p_2} reaches 1350 °C, $M_{23}C_6$ carbides near the grain boundaries undergo precipitation and back-solvation processes, resulting in the fine carbides at grain boundaries, as shown in Fig. 4g. The

microstructures of simulated HAZ with T_{p_1}=T_{p_2}=1450 °C are shown in Fig.4h and 4i. The rapid heating and cooling cannot be conducted due to the equipment restriction, so there is sufficient time for element diffusion inside the matrix during simulation. A large number of microcracks occur on the microstructure at T_{p_2}=1450 °C, indicating that large part of specimen is melted. Because the melting point of C-HRA-2 alloy is 1389 °C, the alloy matrix suffers liquefaction twice after the double-pass welding. Contiguous microcracks appear along the grain boundaries, as shown in Fig.4h, which is due to the sufficient melting of γ matrix during the secondary thermal cycle at high temperatures. Additionally, large-sized particles with size of 2.65 – 3.64 μm can be found inside the grains, as shown in Fig. 4i. EDS results show that the component is composed of Ni, Cr, Co, Mo, and a small amount of C, as shown in Fig.4j and 4k. Besides, the large-sized particles of 8 μm in length and 3 μm in width appear at the grain boundaries, which can be identified as $M_{23}C_6$ carbides due to the high Cr content and relatively low content of other elements. These phenomena all suggest that the matrix liquefies due to the lower heating rate and higher peak temperatures, and the related elements in the matrix, such as Cr and C, have a larger diffusion coefficient and more sufficient time for diffusion in the liquefied phase.

2.4 Grain size and microhardness

The austenite grain sizes in C-HRA-2 alloy under different thermal simulations are shown in Fig.5. The grain size of BM is about 144 μm, which is similar to the austenite grain size under different peak temperatures, indicating that the austenite grains of C-HRA-2 alloy are stable throughout the thermal cycle process. The grain size of simulated HAZ at T_{p_2}=1050 °C is reduced to a certain extent due to the formation of carbides along the grain boundaries, which can act as the pinned grain boundaries, thus inhibiting the grain growth.

HAZ microhardness of C-HRA-2 alloy under different thermal simulations is shown in Fig.6. The microhardness is related to the dissolution amount of solid solute in the matrix, the shape and amount of the precipitate phase, and the area of grain boundaries[26–27]. The microhardness tests cannot be conducted on the specimen under T_{p_1}=T_{p_2}=1450 °C due to the

Element   wt%
C   2.40
Cr   23.42
Co   12.33
Ni   52.02
Mo   9.50
W   0.34

Element   wt%
C   0.93
Cr   22.78
Co   12.40
Ni   56.14
Mo   7.42
W   0.32

Element   wt%
C   2.27
Cr   93.84
Co   0.48
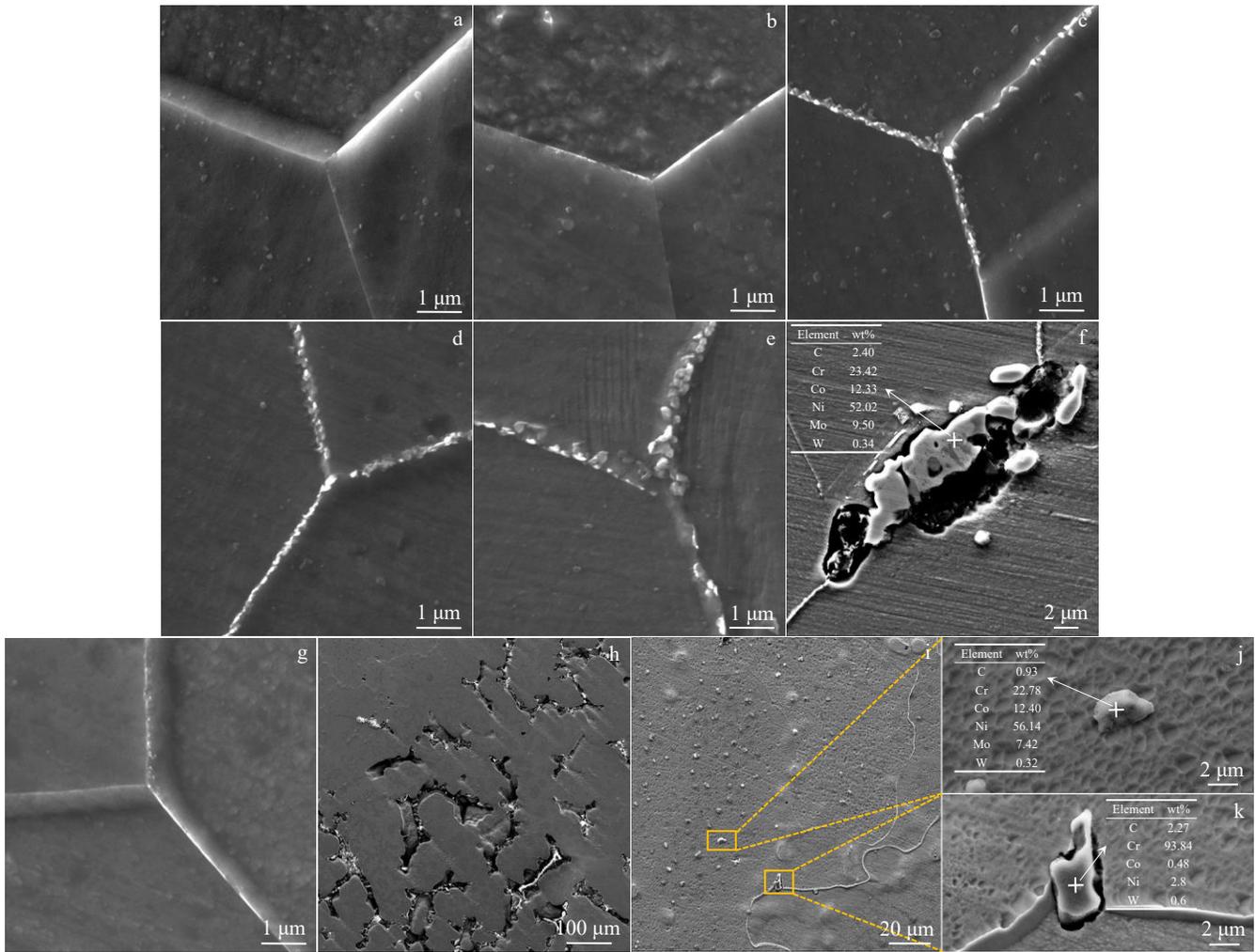Ni   2.8
W   0.6

Fig.4   SEM microstructures near grain boundaries and related EDS analysis results after thermal cycle simulation of double-pass welding at different first and secondary peak temperatures (T_{p_1}/T_{p_2}): (a) 1350 °C/850 °C, (b) 1350°C/950 °C, (c) 1350°C/1050 °C, (d) 1350 °C/1150 °C, (e–f) 1350 °C/1250 °C, (g) 1350 °C/1350 °C, and (h–k) 1450 °C/1450 °C
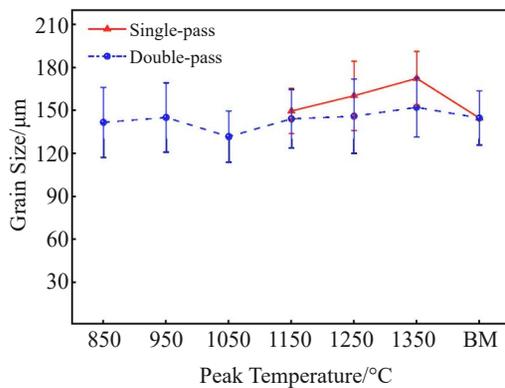

Fig.5   Grain size distributions of HAZ in C-HRA-2 alloy before and after thermal cycle simulation with single-pass and double-pass welding

size restriction. According to Ref. [1, 21], the microhardness HV and yield strength have the specific relationship, as follows:

$$\sigma_y = (2.0–2.2)HV \tag{1}$$

where σ_y is yield strength; HV is microhardness. After analysis, the average microhardness of BM is 452 MPa. The average HAZ microhardness of C-HRA-2 alloy after the single-pass welding and the double-pass welding is 418±8 and 452±25 MPa, respectively. This result indicates that the number of thermal cycles has a strengthening effect on the alloy microhardness, which is consistent with the conclusion in Ref. [13]. T_{p_1} has slight influence on the microhardness of specimen, whereas T_{p_2} has significant effect on the microhardness, indicating that the non-uniformity of grain distribution under the welding thermal simulations leads to a large difference in properties. According to Fig. 6, the microhardness of grain boundaries is basically greater than that of grains, and the overall average microhardness is 485 MPa with T_{p_2}=1250 °C, which is slightly higher than that of BM. The microhardness of specimen under T_{p_2}=1350 °C is the lowest of 412 MPa. This is because the first thermal cycle results in the coarsening of some grain boundaries, as shown in Fig.3d, thereby decreasing the microhardness near the grain
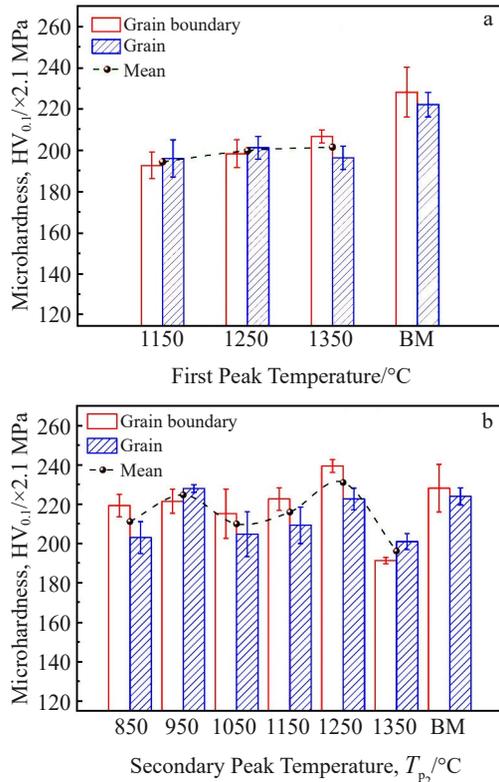
Fig.6 Microhardness of HAZ in C-HRA-2 alloy before and after thermal cycle simulation with single-pass (a) and double-pass (b) welding

boundaries. According to Fig.4g, a few carbides still remain in the grain boundaries of the simulated HAZ with T_{p_2}=1350 °C, resulting in the low microhardness. The overall microhardness of specimen under T_{p_2}=850−950 °C does not change significantly, compared with that of BM. Because the secondary thermal cycle does not satisfy the precipitation condition of $M_{23}C_6$ carbide, the microhardness barely changes. The overall microhardness of specimen under T_{p_2}=1050–1250 °C increases obviously, which is related to the formation of $M_{23}C_6$ carbide near the grain boundaries. The tiny $M_{23}C_6$ carbides can strengthen the grain boundaries, and they are gradually denser near the grain boundaries under T_{p_2}=1050−1250 °C, therefore increasing the microhardness of grain boundaries. However, the overall average microhardness of C-HRA-2 alloy is decreased and then increased due to the weakening of solid solution strength caused by the precipitation of $M_{23}C_6$ carbides.

2.5 Discussion

Based on the abovementioned results, the main influence factor for the precipitation of $M_{23}C_6$ carbides during the secondary thermal cycle is the difference in the solid solution degrees of Cr in the γ matrix obtained at T_{p_1} and T_{p_2}. Based on the Ni-Cr binary equilibrium phase diagram and thermodynamic data in Thermo-Calc software, the equilibrium solid solution degree of Cr in γ(Ni) matrix at 600−1330 °C can be obtained, as follows:

$$\lg [Cr]_\gamma = 1.8610 - \frac{242.8165}{T} \qquad (2)$$

where T is temperature. The solid solution degree of Cr in γ(Ni) is increased with increasing the temperature. The schematic diagrams of the $M_{23}C_6$ carbide precipitation near the grain boundaries during the secondary thermal cycle are shown in Fig.7. Firstly, the double-pass welding results in the saturated Cr in γ matrix. When T_{p_2} is lower than T_{p_1}, the generated content difference causes the migration of Cr atoms to the grain boundaries, and C atoms diffuse rapidly through dislocations and vacancies near the grain boundaries. The number of $M_{23}C_6$ carbides is gradually increased with increasing the T_{p_2}. When T_{p_2} is between 850 and 950 °C, the formation conditions of $M_{23}C_6$ carbides cannot be satisfied. Thus, few carbides appear near the grain boundaries. According to Fig.4c−4e, when T_{p_2} is between 1050 and 1250 °C, Cr in the matrix approaches the vicinity of grain boundaries and combines with the C atoms distributed at the grain boundaries to form $M_{23}C_6$ carbides. Therefore, the number of precipitated $M_{23}C_6$ carbides gradually increases, as indicated by the stage I and stage II in Fig.7. The number of Cr atoms for $M_{23}C_6$ carbide formation is greater than that of C atoms, and the diffusion rate of Cr element at grain boundaries is much greater than that in the grains. Thus, $M_{23}C_6$ carbides are preferentially and continuously precipitated at the locations of C atoms and vacancies on grain boundaries and in regions with higher dislocation density and distortion energy[28]. The diffusion rate of C atoms is higher, so the growth of $M_{23}C_6$ carbides is mainly related to the diffusion of Cr element[29–30]. However, the short holding time at peak temperatures and the subsequent rapid cooling cannot provide sufficient time for the growth of $M_{23}C_6$ carbide precipitate.

When T_{p_1} is elevated to 1250 °C, the carbides near the grain boundaries undergo the precipitation and then re-solution, leading to the fact that no obvious $M_{23}C_6$ carbides can be observed near the grain boundaries. A diffusion zone with a large gradient is generated near the interface between precipitated $M_{23}C_6$ carbides and γ matrix. The re-solution of carbides slows down the concentration gradient in the diffusion zone and partially liquefies this region at peak temperature due to the composition change. Some liquefied phase is transformed immediately into γ matrix at the initial cooling process, and other liquefied phases are solidified to form the microstructure of γ matrix combining with the $M_{23}C_6$ carbide eventually, as shown in Fig.3c and stage III in Fig.7. The $M_{23}C_6$ carbide formed during the first thermal cycle under T_{p_1}=1350 °C is basically dissolved in the secondary thermal cycle. Thus, the composition of transition zone changes, and it is similar to that of γ matrix. The theoretical melting temperature of C-HRA-2 alloy is 1389 °C, which is higher than the peak temperatures. However, the composition change causes the liquefaction of transition zone. The coarsening of grain boundaries occurs due to the liquid phase at grain boundaries, as indicated by the stage IV in Fig.7. When T_{p_2}≥ 1250 °C, the area near the grain boundaries suffers the liquefaction process again, and the liquefaction of γ matrix and the re-solution of $M_{23}C_6$ carbide occur. Afterwards, the microstructure composed of γ matrix and $M_{23}C_6$ carbide is
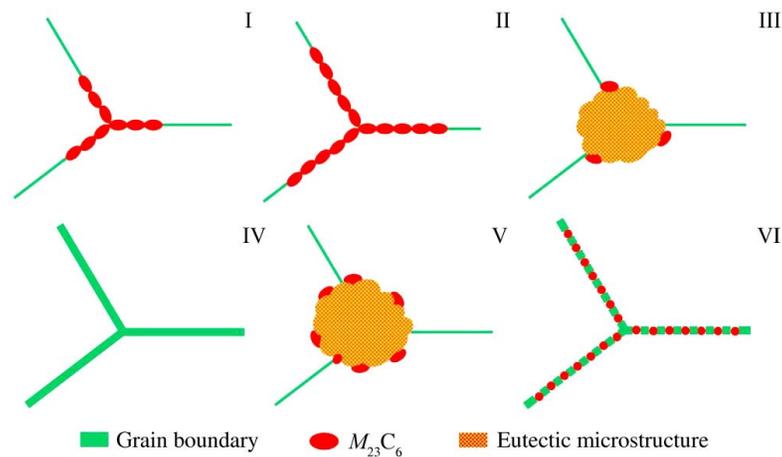
Fig.7   Schematic diagrams of microstructure evolution of $M_{23}C_6$ carbide precipitation near grain boundaries during welding thermal simulation

formed after cooling, as indicated by stage V in Fig. 7. The original molten microstructure is surrounded by many fine granular particles. Grainy bumps can be found along the grain boundaries at 1450 °C in the secondary thermal cycle, as shown in Fig. 4i and indicated by stage VI in Fig. 7. This is mainly because the peak temperature of 1450 °C is higher than the melting point of C-HRA-2 alloy. Thus, the alloy is in the molten state during the secondary thermal cycle under T_{p_2}= 1450 °C. In this case, most γ matrix is transformed into liquid phase at peak temperature, and a large amount of liquid phase remains in the following cooling process due to the slow cooling rate. The grain boundaries migrate, merge, and decrease in this process, and some liquid phase combines with the precipitated large-size granular $M_{23}C_6$ carbides, resulting in the increased granular grain boundaries.

3 Conclusions

1) The size of precipitated $M_{23}C_6$ carbide in the heat-affected zone (HAZ) of C-HRA-2 nickel-based alloy is independent of the number of thermal cycles, but it is related to the peak temperature. The higher the peak temperature, the larger the size of the precipitated $M_{23}C_6$ carbide. After the primary thermal cycle with the first peak temperature T_{p_1}= 1350 °C, Cr is supersaturated around the matrix after cooling, and the precipitation of $M_{23}C_6$ carbide from the γ matrix occurs when the secondary peak temperature $T_{p_2} \geqslant 1050$ °C.

2) The difference in solid solution degree causes the precipitation of $M_{23}C_6$ carbides along the grain boundaries when peak temperature $T_p \geqslant 1050$ °C. When T_p is higher than 1250 °C, the eutectic microstructure formed by γ matrix and $M_{23}C_6$ carbides can be observed near the grain boundaries.

3) The effect of T_{p_2} on grain size is not significant, but the microhardness fluctuates significantly after double-pass welding under different T_{p_2}. The microhardness of C-HRA-2 alloy under T_{p_2}=1250 °C is slightly higher than that of base metal due to the grain boundary strengthening, and the lowest microhardness is caused by the liquefaction of grain boundaries at T_{p_2}=1350 °C. In addition, the number of thermal cycles has a certain strengthening effect on the microhardness

of C-HRA-2 alloy.

References

1   Dong Chen. *Study on Microstructure and Properties of Solid Solution Strengthened Heat Resistant Alloy C-HRA-2*[D]. Beijing: University of Science and Technology Beijing, 2020 (in Chinese)

2   Liu Zhengdong, Chen Zhengzong, He Xikou *et al*. *Acta Metallurgica Sinica*[J], 2020, 56(4): 539 (in Chinese)

3   Liu Z, Guo X Y, Cui H C *et al*. *Materials Science and Engineering A*[J], 2018, 710: 151

4   Dunder M, Samardzic I, Simunovic G *et al*. *International Journal of Simulation Modeling*[J], 2020, 19(2): 209

5   Liu W, Lu F G, Yang R J *et al*. *Journal of Materials Processing Technology*[J], 2015, 225: 221

6   Chen Z Y, Chen Z Z, Kou D X *et al*. *Journal of Iron and Steel Research International*[J], 2022, 29(2): 327

7   Wang X, Wang C, Kang J *et al*. *Materials Science and Engineering A*[J], 2020, 780(C): 139 198

8   Zong Y, Liu C M. *Materials Science Forum*[J], 2018, 913: 317

9   Qi X N, Di H S, Wang X N *et al*. *Journal of Materials Research and Technology*[J], 2020, 9(4): 7838

10 Kanwer S A, Sangeetha R P, Nikhil S *et al*. *International Journal of Pressure Vessels and Piping*[J], 2018, 163: 36

11 Shao Y, Yan B Y, Liu Y H *et al*. *Journal of Manufacturing Processes*[J], 2019, 43(A): 9

12 Fu Ruidong, Lu Yunhai, Yang Yongqiang *et al*. *Transactions of Materials and Heat Treatment*[J], 2007, 97(1): 66 (in Chinese)

13 Zhu Zikun, Han Yang, Zhang Zhou *et al*. *Welding Digest of Machinery Manufacturing*[J], 2022(3):12 (in Chinese)

14 Li S L, Li K J, Cai Z P *et al*. *Journal of Materials Processing Technology*[J], 2017, 258: 38

15 Li S L, Li K J, Cai Z P *et al*. *Metals*[J], 2020, 10(1): 94

16 Jiang He, Ye Jianshui, Dong Jianxin *et al*. *Proceedings of the 13th China Superalloys Conference*[C]. Beijing: The Chinese

Society for Metals, 2015: 226 (in Chinese)

17 Chen Zhengzong, Liu Zhengdong, Liang Baoqi *et al. China Patient*, CN112809242B[P], 2022 (in Chinese)

18 Chen Zhengzong, Liu Zhengdong, Liang Baoqi *et al. China Patient*, CN112846566B[P], 2022 (in Chinese)

19 Chen Zhengzong, Liu Zhengdong, Liang Baoqi *et al. China Patient*, CN112846565B[P], 2022 (in Chinese)

20 Dong C, Liu Z D, Chen Z Z *et al. Journal of Alloys and Compounds*[J], 2020, 825(C): 154 106

21 Dong C, Liu Z D, Wang X T *et al. Journal of Alloys and Compounds*[J], 2019, 821(C): 153 259

22 Dong C, Liu Z D, Chen Z Z *et al. Journal of Iron and Steel Research International*[J], 2020, 27: 820

23 Zhou Gangbao, Bian Shuang, Chen Zhenyu *et al. Journal of Chinese Society of Power Engineering*[J], 2022, 42(5): 475 (in Chinese)

24 He L Z, Zheng Q, Sun X F *et al. Journal of Materials Science*[J], 2005, 40(11): 2959

25 Richards N L, Chaturvedi M C. *International Materials Reviews*[J], 2000, 45(3): 109

26 Peng Yun, Song Liang, Zhao Lin *et al. Acta Metallurgica Sinica*[J], 2020, 56(4): 601 (in Chinese)

27 Quan Chen, Liu Xinbao, Zhu Lin *et al. Heat Treatment of Metals*[J], 2021, 46(6): 135 (in Chinese)

28 Feng Fan, Wang Meiling, Li Zhenhua *et al. Materilas Reports*[J], 2021, 35(9): 9186 (in Chinese)

29 Fang Xudong, Li You, Xu Fanghong *et al. Rare Metal Materials and Engineering*[J], 2021, 50(6): 2091 (in Chinese)

30 Bo Guanghai, Hu Rui, Li Jinshan *et al. Rare Metal Materials and Engineering*[J], 2011, 40(10): 1737 (in Chinese)

焊接热循环及峰值温度对**C-HRA-2**镍基合金组织演变的影响

寇东旭[1]，陈重毅[1]，陈正宗[2]，李永清[3]，麻永林[1]，李一鸣[1,4]

(1. 内蒙古科技大学 材料与冶金学院，内蒙古 包头 014010)

(2. 钢铁研究总院有限公司 特殊钢研究院，北京 海淀 100081)

(3. 内蒙古北方重工集团有限公司 技术中心，内蒙古 包头 014033)

(4. 内蒙古科技大学 内蒙古自治区新金属材料重点实验室，内蒙古 包头 014010)

摘　要：通过焊接热模拟方法得到了C-HRA-2镍基合金在不同一次峰值温度（T_{p_1}=1150，1250，1350 ℃）和二次峰值温度（T_{p_2}=850，950，1050，1150，1250，1350，1450 ℃）下的焊接热影响区（HAZ），研究了峰值温度和热循环次数对C-HRA-2合金HAZ微观组织演变的影响，并测试了其显微硬度。采用光学显微镜、扫描电镜和透射电镜对HAZ的微观结构和碳化物进行表征。结果表明，在T_{p_1}=1150 ℃的HAZ中，可观察到沿晶界析出的细小的$M_{23}C_6$碳化物。在T_{p_1}>1250 ℃的HAZ中，在晶界附近发现由于成分液化而导致的γ基体与$M_{23}C_6$碳化物组成的微观结构。当T_{p_2}在1050~1250 ℃，可在HAZ中的晶界附近观察到与在T_{p_1}=1150 ℃的HAZ中类似结构的碳化物，这是由T_{p_1}和T_{p_2}间基体中Cr的固溶度差值导致的。在T_{p_2}>1250 ℃的HAZ中，在晶界附近可观察到与在T_{p_1}=1250 ℃的HAZ中类似的熔融态微观组织。随着T_{p_2}的升高，显微硬度出现很大程度的起伏，在T_{p_2}=1250 ℃的试样显微硬度要稍高于母材硬度，这是因为晶界附近出现的碳化物起到了晶界强化作用。

关键词：C-HRA-2合金；焊接热模拟；组织演变；$M_{23}C_6$碳化物

作者简介：寇东旭，男，1995年生，硕士生，内蒙古科技大学材料与冶金学院，内蒙古 包头 014010，E-mail：2215149692@qq.com